IET Renewable Power Generation

Research Article

Approach to dynamic voltage stability analysis for DFIG wind parks integration

ISSN 1752-1416
Received on 30th May 2016
Revised 18th September 2017
Accepted on 18th October 2017
E-First on 21st November 2017
doi: 10.1049/iet-rpg.2016.0482
www.ietdl.org

Majid Baa Wafaa[1] ✉, *Louis-A Dessaint*[1]
[1]*Department of Electrical Engineering, École de Technologie Supérieure (ÉTS), Montréal, QC, H3C 1K3, Canada*
✉ *E-mail: Baawafaa3@gmail.com*

Abstract: In this study, an improved voltage stability index that can evaluate the unstable behaviour of the power system with doubly-fed induction generator (DFIG) wind parks integration is presented. Accordingly, voltage stability constrained optimal power flow (VSC-OPF) is studied including an improved impedance-based (IB) index. In particular, this study has two main contributions. First, it proposes an IB index with consideration of DFIG capability curve limits and on-load tap changer (OLTC) behaviour. The proposed voltage stability index can detect precisely the voltage collapse, especially after the occurrence of a given contingency due to the dynamic elements of the system. In this study, a model is proposed for DFIG capability curve limits that can be integrated to the internal circuit of the generator. In particular, the proposed model can be appended to impedance matching theory. Furthermore, the OLTC model is added to this index. The index uses the concept of the coupled single-port circuit. The second contribution proposes a VSCOPF with an improved IB index that is also compared with three existing VSC-OPF methods in stressed and single line outage conditions. These approaches are tested and validated on modified WSCC test system, IEEE 39-bus, IEEE 57-bus and Polish 2746-bus systems.

1 Introduction

Nowadays, voltage stability assessment is an important issue in the power system due to blackouts in different countries [1]. The main goal of the power system operator is to run the power system without any voltage instability at the lowest cost. Voltage stability can be affected by several elements and controllers, which operate on different time scales [2]. In particular, the effects of a wind generator (WG) are undeniable. The WG equipped with induction generator absorbs reactive power. As known, most reasons for voltage collapse are based on failing to provide reactive power demands. Therefore, the proper modelling of the WG and its reactive power limits should be adequately analysed for voltage instability detection [3].

Doubly-fed induction generators (DFIGs) are employed in the most newly installed WG in a modern power system. The wind penetration level has been increased in recent times. Many studies had been carried on DFIG reactive power capability curve [4–8]. The DFIG and converter systems can provide the reactive power capability curve. As an illustration, the authors in [8] have investigated the reactive capability curve of DFIG in the rotor-side converter (RSC) and the grid-side converter (GSC). In [9], the authors show the different types of reactive capability curves in the fully rated converter (FRC), DFIG with RSC support and DFIG with RSC and GSC support. Those papers disregarded to propose a method to detect voltage instability.

Most studies have investigated the WG on short-term voltage stability [8, 10], steady-state voltage stability analysis [11], low-voltage ride through control scheme [12]. The studies still lack a detailed model considering the DFIG reactive power capability characteristics in the long-term voltage stability assessment. They also ignored to consider the dynamic behaviour of over excitation limiter (OEL) and on-load tap changer (OLTC).

In order to detect voltage instability, different voltage stability indices have been proposed in the literature. The roles of these indices lie in the evaluation of voltage instability risk and the prediction of voltage collapse point. Some indices are a minimum singular value (MSV) of the power flow Jacobian, MSV of the reduced Jacobian [13] and L-index [14]. Also, there are several line stability indices that have a close relation with active power, reactive power and the voltage stability [15]. Such indices are namely: voltage collapse proximity indicator (VCPI) [16, 17] and equivalent node voltage collapse index [18]. The above-mentioned indices cannot consider the dynamic behaviour of the power system, especially in post-contingency conditions.

One of the important indices in voltage stability studies is an index based on the impedance matching theorem. Different approaches were presented to calculate Thevenin equivalent impedance (TEI) such as least-squares technique [19], Tellegen's theorem [20], adaptive algorithm [21] and recursive least-squares technique [22]. The above-mentioned methods use two successive phasor measurements to compute TEI, however, Abdelkader and Morrow [23, 24] have implemented, respectively, three and five successive phasor measurements. The impedance calculation has been simplified in [25] by changing the impedance matrix of the power system into the two-bus equivalent system.

A new concept called coupled single-port model was reported in [26]. This concept helps to calculate Thevenin parameters by decoupling the load and generator buses. However, this model suffers from several major drawbacks. Specifically, if the load scenarios increase suddenly or randomly, this model behaves inaccurately. This drawback can be overcome by modified coupled single-port model [27]. This method still cannot detect the voltage instability after the occurrence of a contingency. The comparison of different approaches for the calculation of TEI has been carried out based on accuracy and number of phasor measurement units (PMUs) in [28]. It shows that coupled single-port model is one of the worst models for the voltage stability detection in dynamic studies. Furthermore, this model has not been developed with high penetration of wind parks.

Optimal power flow (OPF) with wind generation has become one of the most wide tools used in the power system planning, operation, and electricity market [29, 30]. However, these studies do not investigate voltage stability constrained OPF (VSC-OPF) with consideration of wind generation. Also, traditional VSC-OPF methods have some disadvantages such as inaccuracy of the voltage instability detection [17, 31–33]. Due to the dynamic behaviour of the power system, VSC-OPF methods should use an appropriate index to properly predict the unstable operating point.

This paper attempts to overcome these aforementioned limitations and presents a comprehensive model to identify proper criteria for voltage stability evaluation and then to combine it with

© The Institution of Engineering and Technology 2017

an OPF while considering the contingency. The main contributions of this paper could be summarised as follows:

i. This study proposes an impedance-based (IB) index that can model the great changes during a voltage collapse process such as line tripping, load tap changing and reactive power limits of DFIG and conventional generator. This index can also monitor online voltage stability.
ii. The proposed IB index can model the DFIG reactive power capability characteristics as a variable virtual impedance which is adaptable in the dynamic studies. Therefore, the model of DFIG reactive limits can be integrated to the internal circuit of the generator and it can be appended to impedance matching theory.
iii. An OLTC model is also added to this index. The OLTC can affect both TEI and load impedance. Thus, the IB index equation is modified by considering those impedance variations on the OLTC model. The robustness of the proposed method has been investigated by including SVC and different load types in the power systems.
iv. A new VSC-OPF is carried out with the proposed IB index. The proposed VSC-OPF can reduce the operating cost and the number of voltage collapses. Thus, it can improve the performance of the electric utilities.

The remaining of this paper is organised as follows. The paper starts with a detailed statement of background in Section 2. The new IB voltage stability index is introduced in Section 3. The VSC-OPF method that combines both the OPF and the proposed index is provided in Section 4. The case studies and simulation results are presented in Section 5, whereas Section 6 draws the conclusion and future works.

2 Background

2.1 Impedance matching theory and its application

An impedance matching is a proper way to estimate the maximum power transferred to a load bus. As known, the TEI is a criterion for the voltage stability assessment. The impedance matching can be determined as

$$|Z_{\rm L}| = |Z_{\rm eq}| \tag{1}$$

where $Z_{\rm L}$ and $Z_{\rm eq}$ are, respectively, the load impedance and the TEI.

The voltage of the Thevenin equivalent circuit can be defined as follows:

$$E_{\rm eq} = V_{\rm L} + I_{\rm L} Z_{\rm eq} \tag{2}$$

where $V_{\rm L}$ and $I_{\rm L}$ are the load voltage and load current, respectively.

As mentioned before, there are many methods to calculate $Z_{\rm eq}$. One of these methods adopts coupled single-port model. In this model, the buses are first divided into generator buses, tie buses and load buses in the admittance matrix ($\boldsymbol{Y}$), which is shown as

$$\begin{bmatrix} I_{\rm L} \\ 0 \\ I_{\rm G} \end{bmatrix} = \begin{bmatrix} Y_{\rm LL} & Y_{\rm LT} & Y_{\rm LG} \\ Y_{\rm TL} & Y_{\rm TT} & Y_{\rm TG} \\ Y_{\rm GL} & Y_{\rm GT} & Y_{\rm GG} \end{bmatrix} \begin{bmatrix} V_{\rm L} \\ V_{\rm T} \\ V_{\rm G} \end{bmatrix} \tag{3}$$

Then, the system equivalent impedance matrix ($\mathbf{Z}_{\rm LL}$) can be expressed as [26]

$$V_{\rm L} = K V_{\rm G} - \mathbf{Z}_{\rm LL} I_{\rm L} \tag{4}$$

$$\mathbf{Z}_{\rm LL} = \left(Y_{\rm LL} - Y_{\rm LT} Y_{\rm TT}^{-1} Y_{\rm TL}\right)^{-1} \tag{5}$$

$$K = \mathbf{Z}_{\rm LL}\left(Y_{\rm LT} Y_{\rm TT}^{-1} Y_{\rm TG} - Y_{\rm LG}\right) \tag{6}$$

Equations (4)–(6) can be reformulated for load bus i as follows [26]:

$$\begin{aligned} V_{{\rm L}i} &= E_{{\rm eq},i} - Z_{{\rm LL}ii} I_{{\rm L}i} - \sum_{j=1, i \neq j}^{n} Z_{{\rm LL}ij} I_{{\rm L}j} \\ &= E_{{\rm eq},i} - Z_{{\rm LL}ii} I_{{\rm L}i} - E_{{\rm coupled},i} \end{aligned} \tag{7}$$

where $E_{{\rm eq},i}$ represents the equivalent voltage on the ith bus and $E_{{\rm coupled},i}$ denotes the coupling effects of other loads on $V_{{\rm L}i}$. $Z_{\rm LL}$ presents the system equivalent impedance and $Z_{{\rm LL}ii}$ is created by the diagonal elements of $Z_{\rm LL}$.

The coupled impedance has been presented via the concept of the coupled single-port circuit. The coupled impedance is determined as follows [26]:

$$Z_{{\rm coupled},i} = \frac{E_{{\rm coupled},i}}{I_{{\rm L}i}} = \sum_{j=1, i \neq j}^{n} Z_{{\rm LL}ij}\left(\frac{I_{{\rm L}j}}{I_{{\rm L}i}}\right) \tag{8}$$

2.2 DFIG capability curve limits

There are different models for the representation of the DFIG capability curve limit in the voltage stability studies. As mentioned before, it can be defined for the DFIG capability curve of the RSC and the GSC. The RSC capability is generally bound by the rotor current, rotor voltage, and stator current limits. These constraints can change with the slip value of the generator. It is assumed GSC is a lossless converter and it has a unity power factor. Thus, the RSC capability curve is only considered in this study.

The equation below represents reactive power limit by rotor current [9]

$$Q_{S\max} = \sqrt{S_{Ir_{\max}}^2 - P_S^2} - \frac{|V_s|^2}{X_m + X_S} \tag{10}$$

$$S_{Ir_{\max}} = \left|I_{r_{\max}}\right| \cdot |V_s| \cdot \left|\frac{X_m}{X_m + X_S}\right| \tag{11}$$

where $Q_{S\max}$ represents the reactive power limit of the stator, $S_{Ir_{\max}}$ is the maximum apparent power and $I_{r_{\max}}$ is the maximum rotor current. X_S and X_m Are respectively the stator leakage and magnetising reactance.

The maximum stator current can be constrained by the thermal limit of stator coils. Thus, another limit of DFIG reactive power is as follows [34]:

$$Q_{S\max} = \sqrt{\left(\left|I_{s_{\max}}\right| \cdot |V_s|\right)^2 - P_S^2} \tag{12}$$

where $I_{s_{\max}}$ represents the maximum stator current.

Since the rotor current limit is usually smaller than the rotor voltage limit, therefore the rotor voltage limit can be disregarded.

2.3 VSC-OPF model

The VSC-OPF solution should satisfy both technical and economic issues, which are the minimisation of the total costs and the consideration of the voltage stability limits. In order to solve the VSC-OPF, at least one extra constraint should be included in the standard formalisation of the OPF and also several supplementary constraints should be added for wind farm integration. The generated active power of wind farms is considered as a control variable. The limits, in this case, are related to the active power, reactive power, voltage, thermal, wind capacity and voltage stability. The costs are defined as linear and quadratic functions for wind and conventional generators, respectively. The first objective function and its limits are defined as follows:

$$\min \sum_{i \in \alpha_{\rm G}} \left(C_{G_i} + C_{Q_i}\right)$$

© The Institution of Engineering and Technology 2017

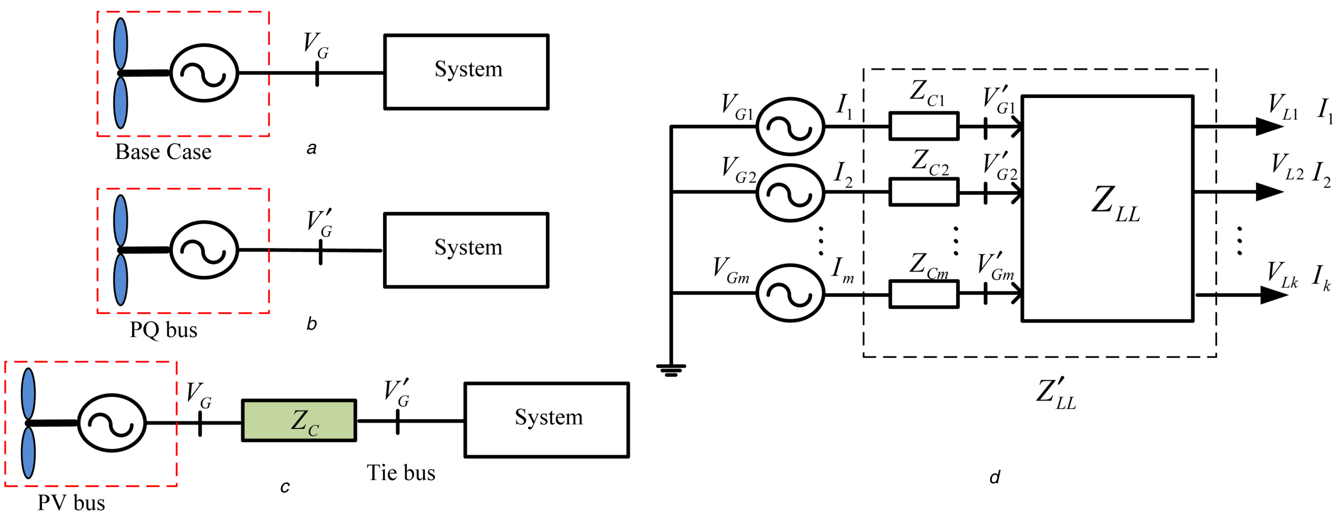

Fig. 1 *Modelling of the DFIG reactive power limit*
(a) Base case, ***(b)*** After DFIG reactive power limit, ***(c)*** Modified system, ***(d)*** Modified multi-port power system with considering proposed model

$$
\begin{aligned}
&\text{s.t.}\quad f(\delta,\ V,\ Q_{\rm G},\ P_{\rm G}, Q_{\rm w}, P_{\rm w}) = 0 \rightarrow \text{PF equation}\\
&P_{G_{\min}} \le P_{\rm G} \le P_{G_{\max}} \rightarrow \ \text{active power limit}\\
&Q_{G_{\min}} \le Q_{\rm G} \le Q_{G_{\max}} \rightarrow \text{reactive power limit}\\
&V_{\min} \le V \le V_{\max} \rightarrow \ \text{voltage limit}\\
&I_{ij}(\delta,\ V) \le I_{ij\max} \rightarrow \text{thermal limit}\\
&C_{\rm w,min} \le C_{\rm w} \le C_{\rm w,max} \rightarrow \text{wind capacity limit}\\
&r_{\rm w,min}C_{\rm w} \le Q_{\rm w} \le r_{\rm w,max}C_{\rm w} \rightarrow \text{wind reactive power limit}\\
&\mathrm{VSI}_{\min} \le \mathrm{VSI} \le \mathrm{VSI}_{\max} \rightarrow \ \text{voltage stability limit}
\end{aligned}
\tag{13}
$$

where $\alpha_{\rm G}$ represents the sets of generator buses; C_{G_i}, C_{Q_i} are the cost functions of the generator i for the generation of the active and the reactive power ($/h). $P_{G_{\min}}$ and $P_{G_{\max}}$ are the minimum and maximum active power generation limits (MW), $Q_{G_{\min}}$ and $Q_{G_{\max}}$ are the minimum and maximum reactive power generation limits (MVAR), $\mathrm{VSI}_{\min}$ and $\mathrm{VSI}_{\max}$ are the minimum and maximum voltage stability index limits and $I_{ij}(\delta,\ V)$ indicates the current in the transmission line between buses i and j $(i \ne j)$. $C_{\rm w,min}$ and $C_{\rm w,max}$ are the minimum and maximum capacity limits of the wind farm (MW) $r_{\rm w,min}$ and $r_{\rm w,max}$ are the minimum and maximum limits in the ratio of reactive power to the capacity of the wind farm $Q_{\rm w}$ is the reactive power of wind farm (MVAR).

As known generated active power of the wind farm ($P_{\rm w}$) depends on wind speed. Hence, $P_{\rm w}$ can be calculated by multiplying the capacity limit by a generation coefficient between [0, 1].

For this study, there are other objective functions that will be introduced later like the minimisation of the VSI (Min (VSI)). where VSI is one of the VSIs.

3 Proposed IB index

In this section, the IB VSI is defined, which can precisely detect the voltage instability. The DFIG reactive power limit and OLTC behaviour are chosen to modify the traditional IB index because of their effects on long-term voltage stability. The traditional IB index can be defined as follows:

$$
\text{Traditional IB}_i = \frac{|Z_{\mathrm{eq},i}|}{|Z_{\mathrm{L}i}|}
\tag{14}
$$

3.1 Model of DFIG reactive limit in improved IB index

In the impedance matching theory, the DFIG reactive limit affects both load impedance and TEI. In this study, the DFIG reactive limit is modelled using a variable virtual impedance in the impedance matching equation. This constraint results in an increased TEI seen at the load bus. Hence, the additional impedance can be appended to this model. Note that due to DFIG and conventional generator reactive limits, it generally increases the risk of voltage instability.

This model is compatible with different operation modes of DFIG, e.g. power factor controlled and voltage controlled mode. To operate in the voltage controlled mode, the DFIG can be modelled as a PV bus, and then it can be considered as a PQ bus when it reaches the reactive power limit. In the power factor controlled mode, DFIG is considered with the unit or specific power factor in normal conditions. However, the DFIG will start to control the reactive power when the terminal voltage drops below a set value in the abnormal conditions.

Fig. 1 shows the model of the DFIG reactive limit. As shown in Fig. 1*a*, the base case of DFIG circuit can become a PV bus (in a voltage controlled mode) and a PQ bus (in a power factor controlled mode) before reaching a reactive limit. The DFIG will be a PQ bus when reaching a reactive power limit as shown in Fig. 1*b* and the DFIG terminal voltage decreases from $V_{\rm G}$ to $V_{\rm G}'$. In other words, an additional impedance Z_C is defined in Fig. 1*c* to model the mentioned limit. Note that a new bus is added as a tie bus to the system.

The modified multi-port system is depicted in Fig. 1*d*, when the reactive power limits are considered for all DFIG generators and Z_C are the virtual impedance of the model of the DFIG reactive limit.

The new equation of the admittance matrix after adding the proposed model is as follows:

$$
\begin{bmatrix} I_{\rm L}\\ 0\\ 0\\ I_{\rm G}\end{bmatrix} = \begin{bmatrix} Y_{\rm LL} & Y_{\rm LT} & Y_{\rm LG} & 0\\ Y_{\rm TL} & Y_{\rm TT} & Y_{\rm TG} & 0\\ Y_{\rm GL} & Y_{\rm GT} & Y_{\rm GG}+Y_{\rm C} & -Y_{\rm C}\\ 0 & 0 & -Y_{\rm C} & Y_{\rm C}\end{bmatrix} \begin{bmatrix} V_{\rm L}\\ V_{\rm T}\\ V_{\rm G}'\\ V_{\rm G}\end{bmatrix}
\tag{15}
$$

where $\boldsymbol{Y}_{\rm C}$ is the diagonal matrix with $((1/Z_{C1}),\ (1/Z_{C2}), \ldots, (1/Z_{Cm}))$ values.

Since the added bus acts as a tie bus, (15) is simplified as

$$
\begin{bmatrix} I_{\rm L}\\ 0\\ I_{\rm G}\end{bmatrix} = \begin{bmatrix} Y_{\rm LL} & Y_{\rm LT}' & 0\\ Y_{\rm TL}' & Y_{\rm TT}' & Y_{\rm TG}'\\ 0 & Y_{\rm GT}' & Y_{\rm C}\end{bmatrix} \begin{bmatrix} V_{\rm L}\\ V_{\rm T}'\\ V_{\rm G}\end{bmatrix}
\tag{16}
$$

The additional impedance can be detailed from the following equation:

$$
Z_{\rm C} = \frac{V_{\rm G} - V_{\rm G}'}{I_{\rm G}}
\tag{17}
$$

© The Institution of Engineering and Technology 2017

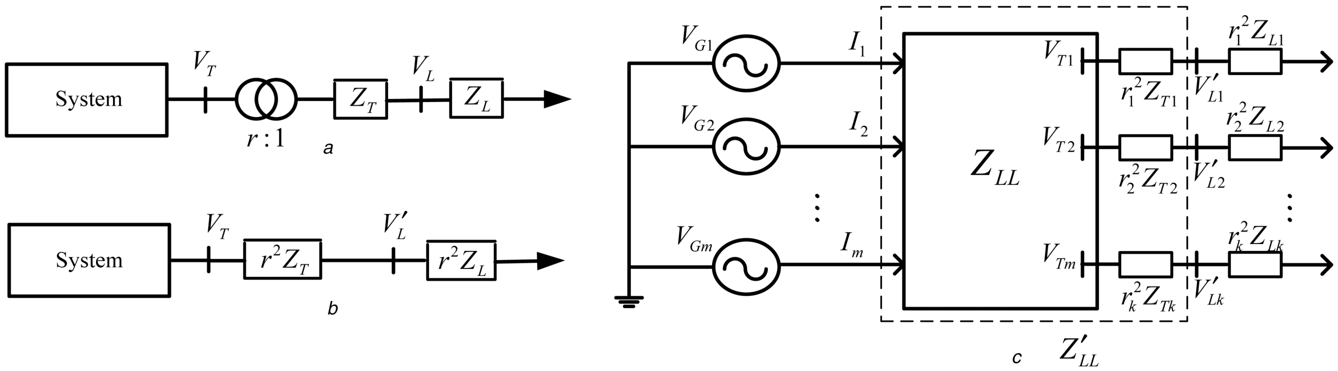

Fig. 2 *Modelling of the OLTC*
(a) System with OLTC, ***(b)*** Modified system, ***(c)*** Modified multi-port power system with considering OLTC model

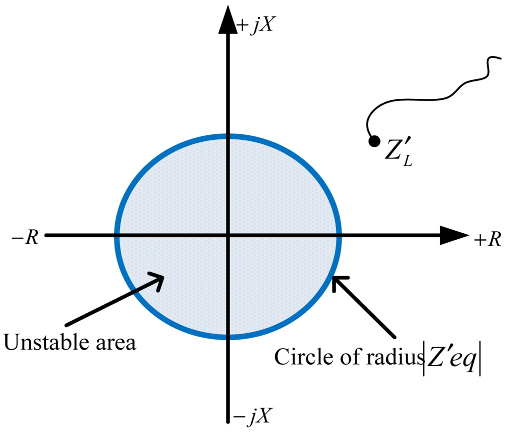

Fig. 3 *Mapping of stability in the R–X diagram for improved IB index*

where V_G and V'_G, respectively, are the generator voltages before and after DFIG reactive limit action.

The DFIG generator gives similar reactive power capability as a conventional generator. Thus, this model is applicable with the reactive power limit of conventional generators.

3.2 OLTC model in improved IB index

In order to present the effect of OLTC on the improved IB index, it is assumed that all OLTCs have the same tap steps and time delay. As shown in Figs. 2*a* and *b*, the effect of OLTC on element impedance is divided into two parts, namely, the OLTC impedance (Z_T) and load impedance (Z_L). Consequently, the IB index equation can be modified.

Fig. 2*c* shows the multi-port system when the OLTC model is considered in the system. It is assumed that OLTC is installed on all loads. As shown, the TEI (Z_{eq}) and the load impedance (Z_L) are modified. The modelling of OLTC can enhance the voltage stability detection.

3.3 Formulation of improved IB index

In the previous sections, the model of DFIG reactive limit and model of OLTC were presented to modify the traditional IB index. For example, the TEI will change as follows:

$$Z'_{eq,i} = Z'_{LLii} + Z_{coupled,i} \tag{18}$$

where $Z_{coupled,i}$ is the coupling effect and Z'_{LLii} which is system equivalent impedance is modified with the effect of these two factors:

i. Virtual impedance due to DFIG reactive power limits (Fig. 1).
ii. Impedance increment due to OLTC model (Fig. 2).

Load impedance also will be modified by only the effect of OLTC, thus it is considered $Z'_{Li} = r_i^2 Z_{Li}$ during availability of OLTC.

Based on the impedance matching theory, when the TEI is matched with load impedance; the system will be unstable. Therefore, $Z'_{eq,i}$ should be equal to Z'_{Li} in voltage instability conditions. It can be conquered that when the value of the improved IB index reaches one, the system will be in a critical mode and it will be unstable. The range of variation of the improved IB index is [0, 1]. The improved IB index can be defined as follows:

$$\mathrm{IB}_i = \frac{|Z'_{eq,i}|}{|Z'_{Li}|} = \frac{|Z'_{LLii} + Z_{coupled,i}|}{|r_i^2 Z_{Li}|} \tag{19}$$

The maximum value of the improved IB index shows the weakest bus and is employed by the proposed VSC-OPF in the next section. To show the behaviour of the proposed IB index in the instability detection, the impedance matching in the *R*–*X* diagram is shown in Fig. 3. If the load impedance (Z'_L) is located inside of the circle with radius $|Z'_{eq}|$, the system is unstable. Considering the circle of radius $|Z'_{eq}|$ as a constant value is not accurate because of the dynamic behaviour of power systems. Thus the TEI is considered variable in the proposed index by the effects of OLTC and DFIG reactive limits.

4 Proposed VSC-OPF method

Due to the dynamic behaviour of power systems, the traditional VSC-OPF methods cannot accurately perform the voltage instability evaluation during OLTC actions and DFIG limits, especially in post-contingency conditions. This paper proposes a new VSC-OPF method that is more practical and realistic. The approach includes a detailed modelling of the DFIG and OLTC. In the proposed voltage stability assessment, the first step is to define the IB VSI. Then, the VSC-OPF is performed including the IB constraint as a voltage stability constraint. This IB constraint is defined as follows:

$$\mathrm{IB}_{max}(\delta,\ V,\ Q_G,\ P_G, Q_w, P_w) \le \mathrm{IB}_c \tag{20}$$

where IB_{max} and IB_c represent the maximum and the critical values of the improved IB index, respectively. IB_{max} can show the weakest transmission bus.

To obtain IB_{max}, the values of the improved IB index should be calculated for all load buses in (19). Then the maximum value of the index, which is named IB_{max} is selected to be used in the optimisation problem. As mentioned before, the bus with the highest value of IB index will be the weakest bus. Generally, setting the critical value is very significant; an improper setting may produce an unfeasible VSC-OPF solution. The critical value is a safety margin of unstable operating points. The active power of some buses will be redispatched, when the value of proposed index increases to the critical value. Note that this value creates a trade-

© The Institution of Engineering and Technology 2017

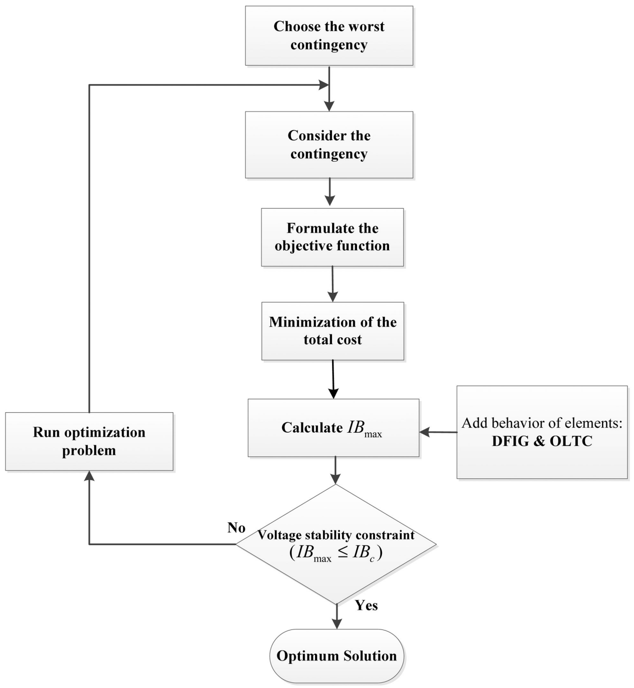

Fig. 4 *Flowchart of the proposed VSC-OPF method*

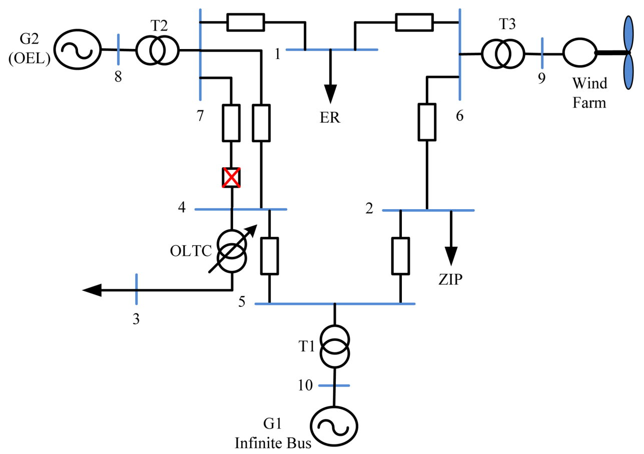

Fig. 5 *Modified WSCC test system*

off between cost and voltage stability issues in the optimisation problem. Several impacts on the definition of critical value in the improved IB index (IB_c) have been presented as follows:

i. Based on the occurrence of contingencies in the past, ISO can define this value.
ii. Analysis of different load dispatches can help to choose the critical value.
iii. N−1 contingency analysis to obtain the worst contingency is a method to define this value accurately.

A flowchart of the proposed VSC-OPF based on the improved IB index is depicted in Fig. 4.

5 Simulation result and discussion

In this section, both dynamic and static studies are performed to demonstrate the effectiveness of the proposed model. They are divided into two parts: voltage stability monitoring and VSC-OPF. Several case studies are selected to verify the results which are detailed as below. The optimisation algorithm which is used in the VSC-OPF is primal-dual interior point method.

Table 1 Transmission line data for modified WSCC test system

Bus number From	To	Resistance, p.u.	Reactance, p.u.	Susceptance, p.u.
1	6	0.0119	0.1008	0.209
1	7	0.0085	0.072	0.149
2	5	0.017	0.092	0.158
2	6	0.039	0.170	0.358
3	4	0.0	0.02618	0.0
4	5	0.01	0.085	0.176
4	7	0.032	0.161	0.306
4	7	0.032	0.161	0.306
5	10	0.0	0.0576	0.0
6	9	0.0	0.586	0.0
7	8	0.0	0.625	0.0

5.1 Voltage stability monitoring

By applying the proposed model, several case studies such as modified WSCC test system and IEEE 39-bus system are tested in PSAT [35]. In order to evaluate the performance of this index, no under-voltage protection or load shedding is considered in this work.

5.1.1 Modified WSCC test system: To analyse the effect of the proposed model on the voltage stability, a modified WSCC test system is used which is a looped network system (see Fig. 5). This system is modified with an extra bus (including an OLTC transformer) and a wind park with DFIGs. ZIP and exponential recovery load models are also added into the system. The bus number is rearranged, respectively, as load buses, tie buses and generator buses, because of the coupled single-port model calculation. An automatic voltage regulator (AVR) and an OEL are installed on the conventional generator and loads will be increased until finding a voltage collapse in dynamic simulation. Note that a line transmission tripping is assumed between buses 4 and 7 (at $t = 5$ s).

The maximum field current of OEL is set to 3.4 p.u. The exponential recovery load is recovered by a time constant. Formulas of static active power (p_s) and transient active power (p_t) in this load are $p_s = p_0(v/v_0)^{\alpha_s}$ and $p_t = p_0(v/v_0)^{\alpha_t}$. In this example, the values of α_s, α_t, p_0 and v_0 consider 2, 1.5, 1.9 p.u. and 1.0 p.u., respectively. Fifty wind generators compose the wind park. Percentage of resistance, active current and active power is considered 33% for each of them in the ZIP load model. Transmission line data for the modified WSCC test system is presented in Table 1.

Tap ratio step (0.02), minimum and maximum tap ratio (between 0.8 and 1.2) and a reference voltage (0.9 p.u.) are the parameters of the OLTC. The nominal wind speed is considered 15 m/s and the Weibull distribution used to model the wind speed. The DFIG operates in the voltage controlled mode. The voltage magnitudes, tap changing, proposed IB index and virtual impedance are depicted in Figs. 6*a*–*d*, respectively.

Fig. 6*a* shows the voltage variations after the occurrence of the contingency, where the system reaches the voltage instability point at 36.4 s. It is assumed that the short-term voltage stability evaluation is ignored. The process of restoration by the OLTC is represented in Fig. 6*b*, which has a negative effect on voltage stability. The comparison between traditional and improved IB indices is evaluated in Fig. 6*c*. The improved IB index with the modified coupled single-port model can predict the voltage instability accurately because the index value reaches 0.999 based on the impedance matching theory. As expected, when the improved IB index reaches 1, this operating point will be the collapse point. Otherwise, Fig. 6*c* demonstrates that the traditional IB index (with coupled single-port model) reaches a value of 0.442 and it cannot detect the voltage collapse point. Therefore, the proposed IB index will improve by 55.7% the voltage instability detection in this case. The DFIG changes from PV bus to PQ bus;

© The Institution of Engineering and Technology 2017

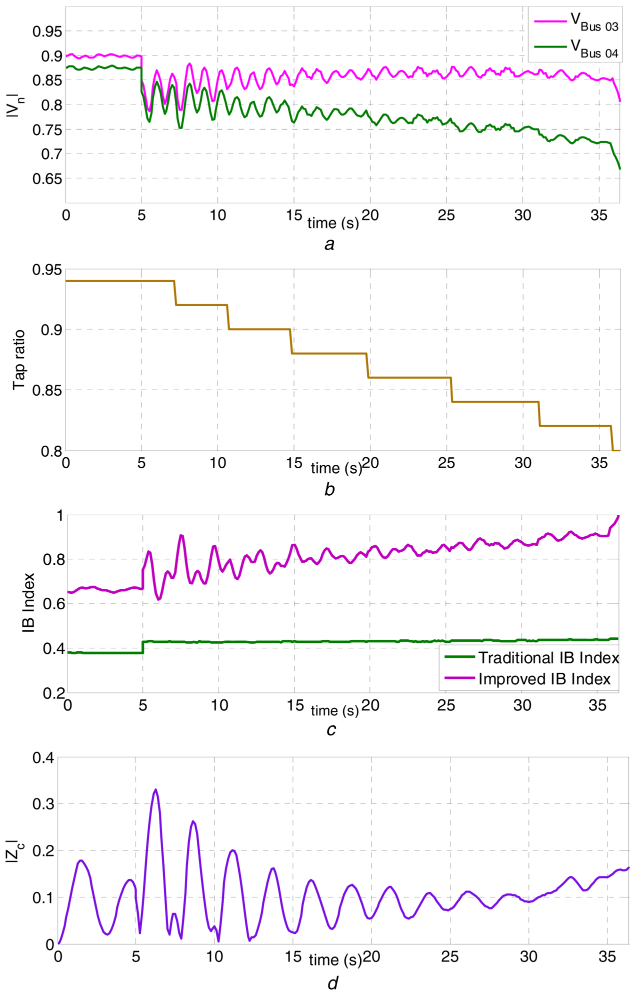

Fig. 6 *Voltage instability in modified WSCC system*
(a) Voltage magnitude at buses 3 and 4, ***(b)*** Tap changing in the OLTC, ***(c)*** Comparison of IB indices at the load, ***(d)*** Virtual impedance of proposed model

therefore, Z_c has a large variation because of the DFIG reactive limit (see Fig. 6*d*). To show the robustness of the proposed method with different load models, ZIP and exponential recovery load model are used in this case.

5.1.2 Modified IEEE 39-bus system: The IEEE 39-bus system that is well known as New-England power system [36] is evaluated in this part. To investigate the performance of the proposed model, a bus with OLTC is added at bus 8 that is called bus number 40 and two wind parks with DFIGs has been added at buses 34 and 37. The nominal wind speed is considered 15 m/s and the Weibull distribution used to model the wind speed. AVR and an OEL are also installed on the conventional generators.

The loading factor of additional bus and other buses has been increased up to 1.3 and 1.6 p.u., respectively. A contingency is considered as a line transmission tripping between buses 8 and 9 ($t = 5$ s). The voltage magnitudes, tap changing, the impedances of the proposed IB index and comparison between traditional and proposed model are presented in Figs. 7*a–d*, respectively.

The results show that extra bus connected to the OLTC (bus 40) is the weakest bus in this case. Because it has higher index value than other buses. Fig. 7*c* shows that the system is collapsing at 61.5 s. As observed, the proposed model can follow unstable behaviour in this case study.

By applying the proposed model, Fig. 7*c* represents the load impedance and the TEI at bus 40. The curves of these two impedances cross each other at the collapse point. Thus, the results are accurate. The impact of the proposed model is presented in Fig. 7*d* that compares the curves of traditional and improved IB index. The traditional IB index reaches a value of 0.708 at the collapse point that shows an optimistic prediction of the voltage

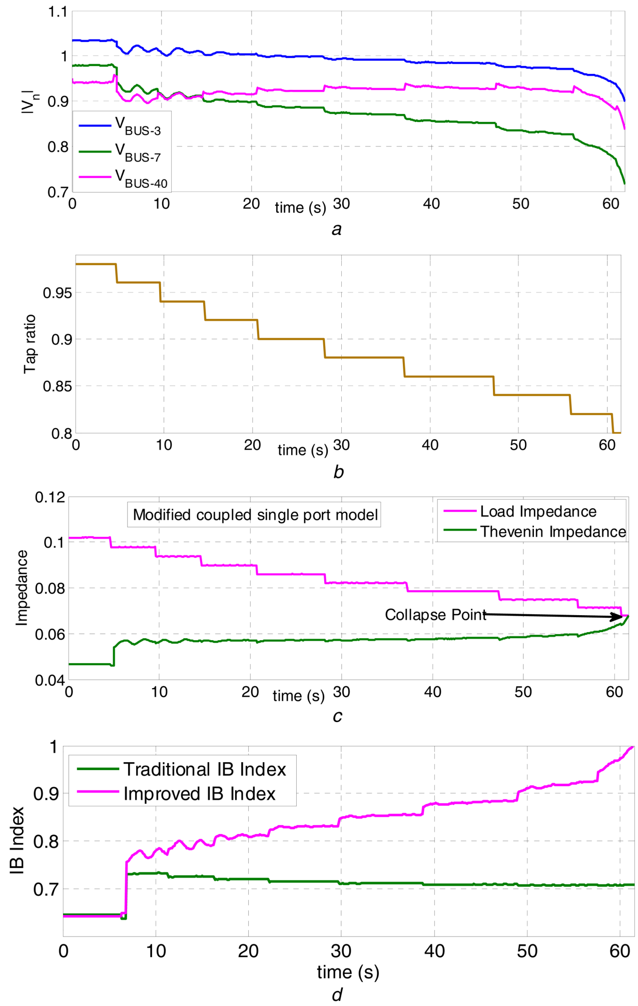

Fig. 7 *Voltage instability in modified IEEE 39-bus*
(a) Voltage magnitude at buses 3, 7 and 40, ***(b)*** Tap changing in the OLTC, ***(c)*** System and load impedances at bus 40, ***(d)*** Comparison between traditional and proposed IB index

instability. Thus, the proposed IB index will improve by 29.1% the voltage instability detection in this case.

To show the robustness of the proposed model, the application of a static var compensator (SVC) has been investigated in this part which is installed in bus 6. As known, SVC increases the voltage stability margin of power systems. Thus, the previous system is stable. To produce a collapse point, the active power of loads and generators will be increased by 15%.

The voltage magnitudes and comparison between traditional and improved index are presented in Figs. 8*a* and *b*, respectively, where the system reaches the voltage instability point at 39.6 s. As shown in Fig. 8*b*, the proposed model can predict the voltage instability accurately.

5.2 VSC-OPF

By applying the proposed model for DFIG wind parks integration, the VSC-OPF is performed in these case studies: IEEE 39-bus, IEEE 57-bus, and Polish 2746-bus systems. All results in this section are carried out in MATPOWER [37]. The comparison has been done between IB-index, L-index, VCPI, and MSV. The VSC-OPF can be carried out with different objective functions as follows:

Case 1: minimise the cost function.
Case 2: minimise the cost function with the extra voltage stability constraint.
Case 3: minimise the index or maximise it, which depends on the type of index.

© The Institution of Engineering and Technology 2017

5.2.1 IEEE 39-bus system: The proposed VSC-OPF method that is OPF combined with improved IB index is presented in Table 1 in the stressed conditions. Loading factor of bus 8 and other buses has been increased to 1.3 and 1.6 p.u., respectively. A line transmission outage is assumed between buses 8 and 9 for single line outage conditions. Also, two wind parks with DFIGs have been added at buses 34 and 37. In case 2, the value of voltage stability constraint should be defined by the independent system operator (ISO). This value is assumed to equal to 0.56 for stressed conditions.

Table 2 can also produce different scenarios with several objective functions and load profiles. Hence, ISO can identify the best strategy in these different scenarios. Where IB_T and IB_{max} are total and maximum VSI between all load buses, respectively, and FC is the fuel cost function. P_w is generated active power of the wind farms. Based on different objective functions, generated wind active power can change in buses 34 and 37.

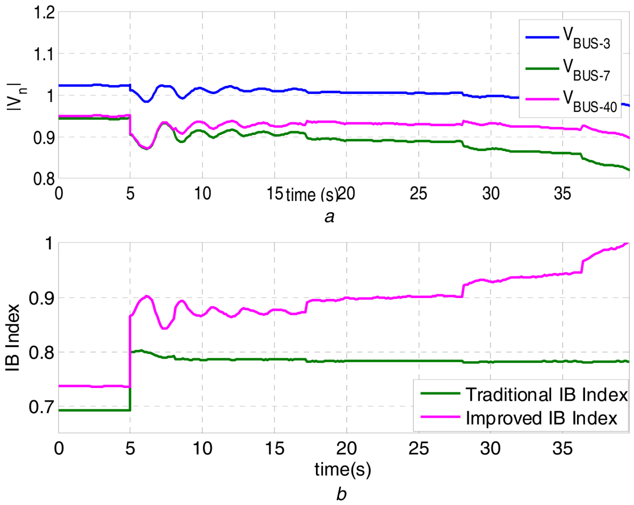

Fig. 8 *Voltage instability in modified IEEE 39-bus with SVC*
(a) Voltage magnitude at buses 3, 7 and 40, ***(b)*** Comparison between proposed and traditional index

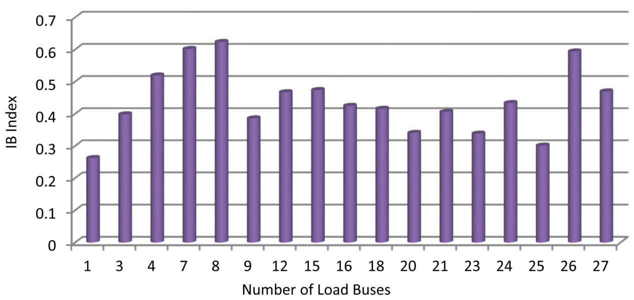

Fig. 9 *Improved IB index values in the IEEE 39-bus system*

In order to minimise the objective function in case 3, improved IB index should be obtained for all load buses. As illustrated in Fig. 9, bus 8 has the maximum value of the index; therefore, it is the weakest bus. Thus, the improved IB index value of bus 8 was selected to be minimised.

5.2.2 IEEE 57-bus system: To compare the proposed VSC-OPF method with other methods, the IEEE 57-bus system is selected to demonstrate the performance of the method. A line transmission outage is considered between buses 8 and 9 for the single line outage conditions. One wind park with DFIGs has been added to bus 12. Fig. 10 shows a comparison between different variables in cases 1, 2 and 3. The fuel cost is the highest in case 3 and it is approximately same in cases 1 and 2. However, case 2 has the lowest generated reactive power and active power losses. This case can satisfy the economic and security issues. It is also seen from Fig. 10 that ISO can find the proper optimal solution from the three objective functions.

The comparison between different VSC-OPF methods is presented in Table 3. The objective functions are as follows: minimise the maximum L-index value (min L_{max}), maximise the MSV (max MSV), minimise total values of VCPI (min $VCPI_T$) and minimise the maximum IB-index value (min IB_{max}). As listed in Table 3, the proposed VSC-OPF (min IB_{max}) has the lowest fuel cost. However, min $VCPI_T$ achieves the lowest generated reactive power and active power losses. This result is due to the fact that VCPI is based on the theory of maximum power transfer between two buses. On the other hand, min $VCPI_T$ has the highest fuel cost. Accordingly, the proposed VSC-OPF has the highest performance between other methods.

5.2.3 Polish 2746-bus system: To validate the proposed VSC-OPF method in the larger system, the Polish 2746-bus system is selected. Forty wind parks with specific reactive power limits have been added into this system. Fig. 11 shows the sorted values of IB indices for all load buses where bus 506 has the maximum value of the index (0.2512); therefore, it is the weakest bus. The improved IB index value of bus 506 is selected to be minimised.

Table 4 shows the comparison between two scenarios with two critical values of the improved IB index. When VSC-OPF is applied, the generated power system is re-dispatched. The process

Table 2 Proposed VSC-OPF results for stressed condition (IEEE 39-bus)

	Objective functions		
	Case 1	Case 2	Case 3
P_w, MW	1393.6	1394.0	1386.2
IB_{max}	0.572	0.56	0.558
IB_T	4.09	4.07	3.48
FC, $/h	108897.48	109562.30	124462.73

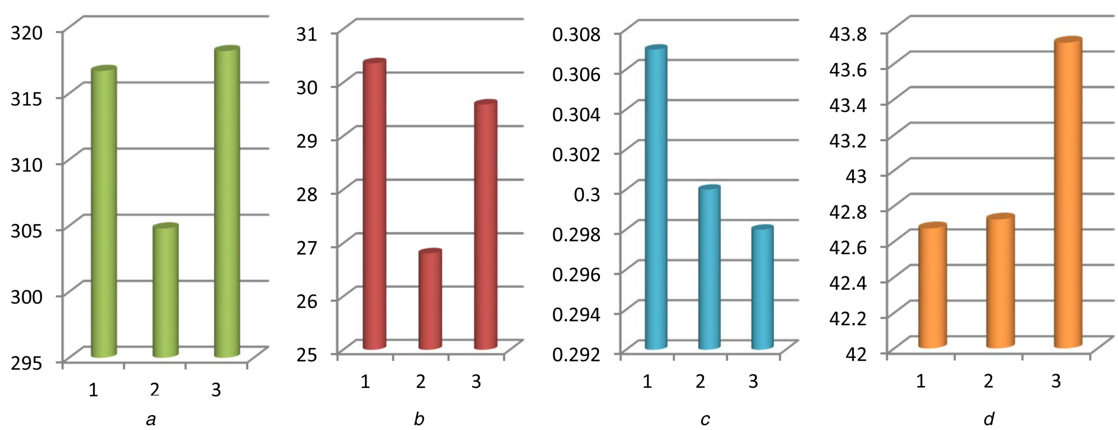

Fig. 10 *Comparison between different variables in IEEE 57-bus system*
(a) Generated reactive power (MVAR), ***(b)*** Active power losses (MW), ***(c)*** Maximum values of improved IB index, ***(d)*** Fuel cost function (K$/h)

© The Institution of Engineering and Technology 2017

Table 3 Comparison between different VSC-OPF results for IEEE 57-bus system (single-line outage condition)

	Objective functions			
	Min L_{max}	Max MSV	Min $VCPI_T$	Min IB_{max}
P_{loss}, MW	37.02	36.97	15.99	29.59
Q_{gen}, MVAR	341.4	342.6	269.2	318.2
IB_{max}	0.304	0.310	0.298	0.298
IB_T	5.398	5.497	5.252	5.3347
FC, $/h	43793.96	43832.90	47265.84	43718.50

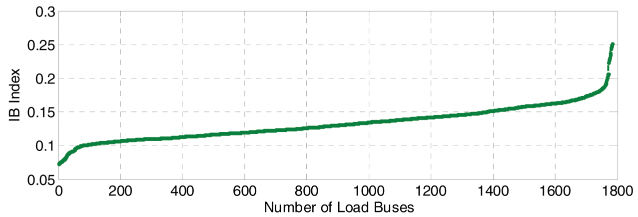

Fig. 11 *Sorted improved IB index values in the Polish 2746-bus system*

Table 4 Proposed VSC-OPF for Polish 2746-bus system

Scenarios	Base case (IB = 0.2512)	IB VSC-OPF (IB = 0.2510)
Objective function, K $/h	1307.88	1308.84

of voltage stability improvement represents that the fuel cost increases, however, the power system has a better voltage stability margin. The ISO can manage the active and reactive generated power.

6 Conclusion

In this paper, we propose the improved IB VSI, which can detect precisely the voltage instability with high penetration of wind turbine. This index can model the DFIG reactive power limit and it uses the concept of the coupled single-port circuit. A VSC-OPF is carried out with the proposed index. The improved model is based on a variable virtual impedance and it is adaptable with DFIG reactive behaviour. The paper proposes also the modelling of the OLTC in the IB index if it is available in the system.

Several dynamic and static studies are proposed to demonstrate the effectiveness of the proposed model. They have been divided into two parts that are voltage stability monitoring and VSC-OPF. By applying the proposed model to voltage stability monitoring, the accurate voltage instability detection has been depicted in three case studies. In particular, the comparison between improved and traditional IB index represents the method performance. The proposed VSC-OPF also has been compared between improved IB-index, L-index, VCPI and MSV. The results reveal that the improved IB index has the lowest operating cost. The results can also produce different scenarios with several objective functions and load profiles. Hence, ISO can identify the proper strategy in these different scenarios. In future works, this VSC-OPF could consider the characteristics of an electricity market such as reactive power market. Therefore, it would be compatible with the electricity market regulations.

7 References

[1] McLinn, J.: 'Major power outages in the US, and around the world,' IEEE Reliability Society, 2009

[2] Canizares, C.A.: 'Voltage stability assessment: concepts, practices and tools'. Power System Stability Subcommittee Special Publication IEEE/PES, final document (thunderbox. uwaterloo. ca/~ claudio/claudio. html# VSWG), 2002

[3] Youssef, E., Azab, R.M.E., Amin, A.M.: 'Comparative study of voltage stability analysis for renewable energy grid-connected systems using PSS/E'. SoutheastCon 2015, 2015, pp. 1–6

[4] Engelhardt, S., Erlich, I., Feltes, C., *et al.*: 'Reactive power capability of wind turbines based on doubly fed induction generators', *IEEE Trans. Energy Convers.*, 2011, **26**, pp. 364–372

[5] Lund, T., Sørensen, P., Eek, J.: 'Reactive power capability of a wind turbine with doubly fed induction generator', *Wind Energy*, 2007, **10**, pp. 379–394

[6] Konopinski, R.J., Vijayan, P., Ajjarapu, V.: 'Extended reactive capability of DFIG wind parks for enhanced system performance', *IEEE Trans. Power Syst.*, 2009, **24**, pp. 1346–1355

[7] Meegahapola, L., Littler, T., Perera, S.: 'Capability curve based enhanced reactive power control strategy for stability enhancement and network voltage management', *Int. J. Electr. Power Energy Syst.*, 2013, **52**, pp. 96–106

[8] Kayikci, M., Milanovic, J.V.: 'reactive power control strategies for DFIG-based plants', *IEEE Trans. Energy Convers.*, 2007, **22**, pp. 389–396

[9] Londero, R.R., Affonso, C.d.M., Vieira, J.P.A.: 'Long-term voltage stability analysis of variable speed wind generators', *IEEE Trans. Power Syst.*, 2015, **30**, pp. 439–447

[10] Meegahapola, L.G., Littler, T., Flynn, D.: 'Decoupled-DFIG fault ride-through strategy for enhanced stability performance during grid faults', *IEEE Trans. Sustain. Energy*, 2010, **1**, pp. 152–162

[11] Vittal, E., Malley, M.O., Keane, A.: 'A steady-state voltage stability analysis of power systems with high penetrations of wind', *IEEE Trans. Power Syst.*, 2010, **25**, pp. 433–442

[12] Xie, D., Xu, Z., Yang, L., *et al.*: 'A comprehensive LVRT control strategy for DFIG wind turbines with enhanced reactive power support', *IEEE Trans. Power Syst.*, 2013, **28**, pp. 3302–3310

[13] Lof, P.A., Andersson, G., Hill, D.J.: 'Voltage stability indices for stressed power systems', *IEEE Trans. Power Syst.*, 1993, **8**, pp. 326–335

[14] Kessel, P., Glavitsch, H.: 'Estimating the voltage stability of a power system', *IEEE Trans. Power Deliv.*, 1986, **1**, pp. 346–354

[15] Guo-yun, C., Luo-nan, C., Aihara, K.: 'Power system voltage stability assessment based on branch active powers', *IEEE Trans. Power Syst.*, 2015, **30**, pp. 989–996

[16] Moghavvemi, M., Faruque, O.: 'Real-time contingency evaluation and ranking technique', *IEE Proc. Gener. Transm. Distrib.*, 1998, **145**, pp. 517–524

[17] Zabaiou, T., Dessaint, L.A., Kamwa, I.: 'Preventive control approach for voltage stability improvement using voltage stability constrained optimal power flow based on static line voltage stability indices', *IET Gener. Transm. Distri.*, 2014, **8**, pp. 924–934

[18] Wang, Y., Li, W., Lu, J.: 'A new node voltage stability index based on local voltage phasors', *Electr. Power Syst. Res.*, 2009, **79**, pp. 265–271

[19] Vu, K., Begovic, M.M., Novosel, D., *et al.*: 'Use of local measurements to estimate voltage-stability margin', *IEEE Trans. Power Syst.*, 1999, **14**, pp. 1029–1035

[20] Smon, I., Verbic, G., Gubina, F.: 'Local voltage-stability index using Tellegen's theorem', *IEEE Trans. Power Syst.*, 2006, **21**, pp. 1267–1275

[21] Corsi, S., Taranto, G.N.: 'A real-time voltage instability identification algorithm based on local phasor measurements', *IEEE Trans. Power Syst.*, 2008, **23**, pp. 1271–1279

[22] Tobón, V.J.E., Gutiérrez, R.E.C., Ramirez, J.M.: 'Voltage collapse detection based on local measurements', *Electr. Power Syst. Res.*, 2014, **107**, pp. 77–84

[23] Abdelkader, S.M., Morrow, D.J.: 'Online tracking of Thevenin equivalent parameters using PMU measurements', *IEEE Trans. Power Syst.*, 2012, **27**, pp. 975–983

[24] Abdelkader, S.M., Morrow, D.J.: 'Online Thevenin equivalent determination considering system side changes and measurement errors', *IEEE Trans. Power Syst.*, 2015, **30**, pp. 2716–2725

[25] Lee, D.H.A.: 'Voltage stability assessment using equivalent nodal analysis', *IEEE Trans. Power Syst.*, 2015, **31**, pp. 1–10

[26] Yunfei, W., Pordanjani, I.R., Weixing, L., *et al.*: 'Voltage stability monitoring based on the concept of coupled single-port circuit', *IEEE Trans. Power Syst.*, 2011, **26**, pp. 2154–2163

[27] Jian-Hong, L., Chia-Chi, C.: 'Wide-area measurement-based voltage stability indicators by modified coupled single-port models', *IEEE Trans. Power Syst.*, 2014, **29**, pp. 756–764

[28] Haoyu, Y., Fangxing, L.: 'A comparative study of measurement-based Thevenin equivalents identification methods'. North American Power Symp. (NAPS), 2014, 2014, pp. 1–6

[29] Jabr, R.A., Pal, B.C.: 'Intermittent wind generation in optimal power flow dispatching', *IET. Gener. Transm. Distrib.*, 2009, **3**, pp. 66–74

[30] Xie, L., Chiang, H.D., Li, S.H.: 'Optimal power flow calculation of power system with wind farms'. 2011 IEEE Power and Energy Society General Meeting, 2011, pp. 1–6

[31] Avalos, R.J., Canizares, C.A., Anjos, M.F.: 'A practical voltage-stability-constrained optimal power flow'. Power and Energy Society General Meeting – Conversion and Delivery of Electrical Energy in the 21st Century, 2008, 2008, pp. 1–6

[32] Milano, F., Canizares, C.A., Invernizzi, M.: 'Voltage stability constrained OPF market models considering *N*−1 contingency criteria', *Electr. Power Syst. Res.*, 2005, **74**, pp. 27–36

[33] Lage, G.G., da Costa, G.R.M., Canizares, C.A.: 'Limitations of assigning general critical values to voltage stability indices in voltage-Stability-Constrained optimal power flows'. 2012 IEEE Int. Conf. Power System Technology (POWERCON), 2012, pp. 1–6

[34] Anaya-Lara, O., Jenkins, N., Ekanayake, J., *et al.*: '*Wind generation, modeling and control*' (Wiley, New York, NY, USA, 2009)

[35] Milano, F.: 'An open source power system analysis toolbox', *IEEE Trans. Power Syst.*, 2005, **20**, pp. 1199–1206

[36] Athay, T., Podmore, R., Virmani, S.: 'A practical method for the direct analysis of transient stability', *IEEE Trans. Power Appar. Syst.*, 1979, **PAS-98**, pp. 573–584

[37] Zimmerman, R.D., Murillo-Sánchez, C.: MATPOWER. Available at: http://www.pserc.cornell.edu//matpower/

© The Institution of Engineering and Technology 2017